Viscoelastic fluid response can increase the speed and efficiency of a free swimmer

Joseph Teran

Department of Mathematics, University of California, Los Angeles, CA 90095

Lisa Fauci

Department of Mathematics, Tulane University, New Orleans, LA 70018

Michael Shelley

Applied Math Lab, Courant Institute, New York University, New York, NY 10012

(Dated: November 11, 2009)

Microorganisms navigate through complex environments such as biofilms and mucosal tissues and tracts. To understand the effect of a complex medium upon their locomotion, we investigate numerically the effect of fluid viscoelasticity on the dynamics of an undulating swimming sheet. First, we recover recent small-amplitude results for infinite sheets that suggest that viscoelasticity impedes locomotion. We find the opposite result when simulating free swimmers with large tail undulations, with both velocity and mechanical efficiency peaking for Deborah numbers near one. We associate this with regions of highly stressed fluid aft of the undulating tail.

Mammalian spermatozoa encounter complex, non-Newtonian fluid environments as they make their way through the female reproductive tract. The successful sperm must swim through cervical mucus, progress through narrow, mucus-containing lumen in the oviduct, as well as eventually penetrate the cumulus layer of the oocyte complex [1, 2]. Viscous environments that contain suspended microstructures are also encountered by bacterial cells as they migrate through biofilms or mucosal tissues [3]. Microorganism motility has motivated research in biological fluid dynamics for more than half a century, beginning with G.I. Taylor's classical analysis of swimming by an infinite sheet [4]. While much progress has been made in understanding the fundamental physics of bacterial and flagellar motion in a Newtonian fluid, the fundamental physics of microorganism motility in a non-Newtonian fluid, even with a prescribed beat form, is only beginning to be uncovered [5–7].

Relating complex biological fluids to viscoelastic fluid models can be difficult. A wide range of relaxation times (1-10s), elastic moduli (0.1-10Pa), and viscosities (0.1-10Pa s), have been reported for cervical mucus (see Lauga [5]). In a very recent study of sperm motility in high viscosity medium, Smith *et al.* [8] re-examines the data of Wolf *et al.* [9] for cervical mucus and estimates a yet lower relaxation time of 0.03s. When combined with reported sperm beat frequencies of 10-50Hz this gives an $O(1)$ or higher estimate of the Deborah number.

For the idealized cases of small amplitude undulations of an infinite sheet [5] and an infinite waving cylinder [7] in fading-memory viscoelastic fluids, it has been shown that swimming speeds are decreased by viscoelastic effects relative to a Stokesian Newtonian fluid. These simple swimmers, with no beginning or end, introduce restrictive symmetry to the coupling of fluid and body. Motivated by sperm flagella which, due to decreased microtubule sliding near the base of the axoneme, swim with accentuated amplitude at the distal (tail) end, we study a freely swimming *finite* sheet immersed in a Stokes Oldroyd-B fluid and having a preferred kinematic sinusoidal geometry. Our numerical approach is based on the immersed boundary method [10], and is validated by comparison with the small-amplitude analysis of Lauga [5] for an infinite sheet. In fact, our calculations show that his analytical results agree very well with the full system even for large amplitude waves. However, for swimming "free" sheets (i.e., with free head and tail) we find that for accentuated tail motions the swimmer moves more quickly and efficiently at $O(1)$ Deborah numbers than does the corresponding swimmer in a Newtonian fluid. This is the regime where the relaxation time of the fluid matchs the stroke frequency of the swimmer. This result is opposite that for infinite sheets, and the difference lies, we believe, in the appearance of regions of highly strained viscoelastic fluid sitting aft of the free swimmer's tail. This stress concentration appears to restrict backwards slippage of the free swimmer during parts of its stroke, thus increasing the average speed. We also study the development of viscoelastic stresses in the approach to steady swimming.

The model This is a coupled fluid-body system: the body shape dynamics and motion induce fluid stresses. These create the fluid velocity that moves the body and may also interact with the shape dynamics. Consider a flexible sheet of length L, immersed in a 2D fluid, along which moves a wave of shape deformation with temporal period τ_f. For an incompressible Stokesian flow, the fluid stress tensor $\mathbf{S}$ and velocity $\mathbf{u}$ satisfy $\nabla \cdot \mathbf{S} = \mathbf{0}$ and $\nabla \cdot \mathbf{u} = 0$. To describe the fluid, we employ the Oldroyd-B (OB) viscoelastic model [11] for which $\mathbf{S} = \mathbf{S}_N + \mathbf{S}_p$, with $\mathbf{S}_N$ the usual Newtonian stress tensor and $\mathbf{S}_p$ the extra stress generated by the transport and distension of an immersed polymer field. In adimensional form after scaling lengths by L and time by τ_f, the fluid is described

by the Stokes-OB equations:

$$-\nabla p + \Delta \mathbf{u} = -\beta \nabla \cdot \mathbf{S}_p + \mathbf{f} \;\; \& \;\; \nabla \cdot \mathbf{u} = 0, \qquad (1)$$

$$De \, \mathbf{S}_p^\nabla = -(\mathbf{S}_p - \mathbf{I}), \qquad\qquad (2)$$

with $\mathbf{S}^\nabla \equiv \partial \mathbf{S}_p / \partial t + \mathbf{u} \cdot \nabla \mathbf{S}_p - \left(\nabla \mathbf{u} \, \mathbf{S}_p + \mathbf{S}_p \, \nabla \mathbf{u}^T \right)$ the upper convected time derivative. Here $De = \tau_p / \tau_f$ is the *Deborah number*, with τ_p the polymer relaxation time. The parameter β measures the relative contribution of the polymeric stress to momentum balance. The product $\beta \cdot De$ is the ratio of polymer to solvent viscosity so that given a particular working fluid, its value is fixed independent of experimental conditions. For either β fixed or $\beta \cdot De$ fixed, the limit $De \to 0$ yields a Newtonian fluid, in the first case with unit dimensionless viscosity, and in the second, with viscosity $1 + \beta De$.

The immersed sheet, Γ, is taken to be a (nearly) inextensible surface along which a traveling bending wave is moving. The sheet position is given by $\mathbf{X}(s,t)$, with s both the arclength and material coordinate. To produce a shape change, the sheet is taken to be a generalized Euler elastica whose elastic energy is given by $\mathcal{E} = \mathcal{E}_{bend} + \mathcal{E}_{tens}$ where

$$\mathcal{E}_{bend} = \frac{E}{2} \int_0^1 \left(\kappa(s) - \bar{\kappa}(s,t) \right)^2 ds \qquad (3)$$

Here $\bar{\kappa}$ is a specified target curvature, the pursuit of which drives the dynamics, and E is an adimensional rigidity, which helps set the time-scale for that pursuit. A tensile energy $\mathcal{E}_{tens}$ is also included and its multiplier is set sufficiently high that stretching and compression between material points is severely limited, making the sheet effectively inextensible. The sheet couples to the fluid through two conditions. The first is that the elastic and tensile energies generate a stress jump within the fluid across Γ. That is, $[\mathbf{S}|_\Gamma \cdot \hat{\mathbf{n}}] = \mathbf{g}$ where $\hat{\mathbf{n}}$ is the upward normal to Γ, and $\mathbf{g}$ is a stress generated variationally from the energy as $\mathbf{g} = -\delta \mathcal{E} / \delta \mathbf{X}$. The second requirement is the no-slip and kinematic boundary conditions, that specify that the velocity $\mathbf{u}_\Gamma$ of the sheet is equal to the fluid velocity on either side of the sheet, that is, $\mathbf{u}_\Gamma(s,t) = \mathbf{u}^+(\mathbf{X}(s,t),t) = \mathbf{u}^-(\mathbf{X}(s,t),t)$.

To solve this system numerically we follow the approach of Fauci *et al.* [12], who first used the immersed boundary method to study sheets swimming in a Newtonian fluid. We simulate both sheets that are spatially periodic, so as to compare with previous analytical results, and "free swimmers".

Results We first check our numerical results against the small-amplitude analysis of Lauga ([5]; see also Fu *et al.* [7] for a related analysis) who considered a periodic sheet immersed in an Stokes-OB fluid. Lauga showed, as Taylor did for a Newtonian fluid [4], that swimmer speed scales with the square of wave amplitude. Further, Lauga showed that the ratio $R(De)$ of the "OB swimmer" speed to that in the Newtonian fluid is always less than one, i.e.,
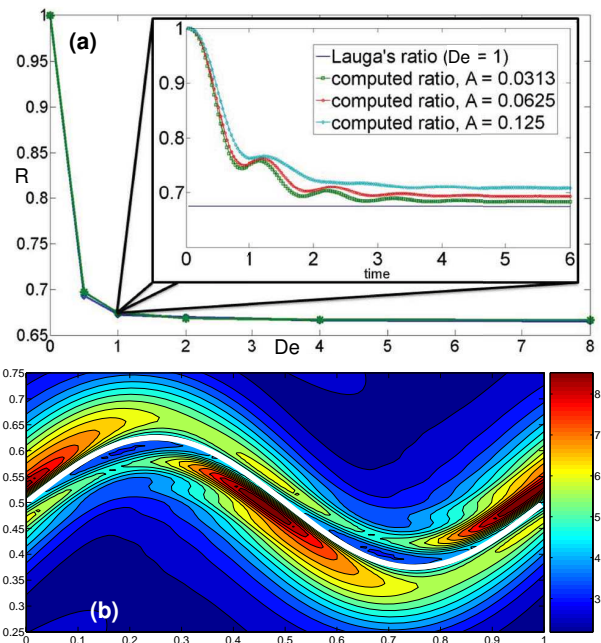
FIG. 1: (a): The speed ratio $R(De) = \mathbf{U}_{OB}/\mathbf{U}_{Newt}$. The green curve is that from long-time numerical simulation, and the blue curve is the theoretical prediction of Lauga [5]. The inset shows the temporal relaxation of this ratio from our simulations for three different wave amplitudes. (b): A periodic sheet swimming to the right in a viscoelastic fluid with $De = 1$ and amplitude $A = 0.125$, simulated to long times. The contours are of $tr(\mathbf{S}_p)$.

the OB swimmer is always slower. To compare, we simulated a spatially periodic sheet with target curvature $\bar{\kappa}(s,t) = -Ak^2 \sin(ks - \omega t)$, where k was chosen so that periodicity was satisfied. The initial polymeric stress was taken as isotropic ($\mathbf{S}_p \equiv \mathbf{I}$). The dynamics was then simulated to long times when the dynamics became steady.

We recover Lauga's asymptotic results in detail. For a small-amplitude swimmer at various De, Fig. 1a shows the computed speed ratio $R(De)$ in comparison with Lauga's formula (for this test we set $\beta De = 1/2$). We also recover the approach of swimmer speed to its time-asymptotic value. This is shown in the inset of Fig. 1a for $De = 1$ as wave amplitude is varied. This shows the relaxational dynamics is oscillatory, and that the deviation of time-asymptotic speed from the limiting ratio is linear in amplitude, as expected. Figure 1b shows the late-time distribution of stress – here contours of $tr(\mathbf{S}_p)$ – around the swimmer ($tr(\mathbf{S}_p)$ represents the mean-square distension of the immersed polymer coils). We also find that as the wave amplitude is increased out of the small-amplitude regime, the ordering of Newtonian swimmer speed to OB swimmer speed is maintained, with the Newtonian swimmer the faster.

We find very different behavior for "free" swimmers executing large-amplitude deformations. Being freed from the constraint of periodicity for the sheet, there is a broader range of possible stroke dynamics. Here we illustrate with simulations using $\bar{\kappa}(s,t) = -Ak^2(s -$
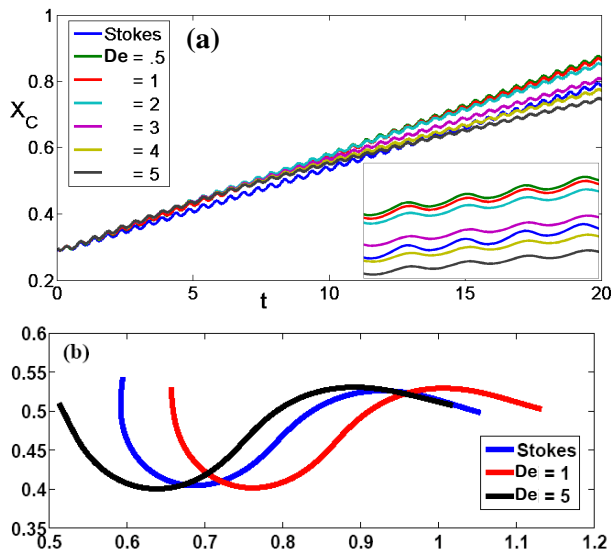
FIG. 2: (a): The location of the x-component of the free swimmer center of mass, with $A = 0.05$, as a function of time for various values of De. The initial displacements are the same for all cases as $\mathbf{S}_0 = \mathbf{I}$. The final time is 20, or $4 \cdot De$ for the largest value of De. (b): The shapes and displacement of three swimmers – $De = 0$ (Newtonian), 1.0, and 5.0 – after 20 periods.

1)$\sin(ks - \omega t)$, which produces a left-moving traveling wave that is of increasing amplitude towards the tail. Figure 2a shows for $A = 0.05$, the horizontal displacement of the center of mass for free swimmers as De is varied, and β held fixed at $1/2$. While the net displacement per stroke is always rightwards, note that the swimmer has a period of backward displacement, unlike the infinite sheet. Since the initial polymeric stress distribution was again isotropic, the initial fluidic response to swimmer motion is Newtonian and the swimmers all have the same initial velocity. However, as the polymeric stresses develop, the OB swimmers accelerate, and the Newtonian swimmer emerges as the slower at intermediate times. From there, the OB swimmers each relax to steady swimming on an $O(De)$ time-scale, and a new ordering emerges as is apparent from the displacement curves (we run the simulations to at least $t = 4De$). At long times, the $De = 1$ swimmer emerges as the fastest, being about 25% faster than the Newtonian swimmer.

The steady-state velocity ratio (relative to Newtonian) is plotted in Fig. 4a, for both β held fixed at $1/2$, and for $\beta De = 1/2$. In either case, the velocity shows a peak around $De = 1$ and a monotonic decrease for larger De. As De is a dimensionless time-scale for the decay of viscoelastic stresses, it is interesting to note that the maximum speed emerges when the Deborah number is matched to the period of the swimming stroke. Swimmer speeds are expected to decay at large De (at least for fixed β) since as $De \rightarrow \infty$ the elastic stresses have no decay time-scale. In that limit, the elastic stress depends upon material strain relative to its initial configu-

ration. Hence, the stretching of material elements caused by a body progressing forward will ultimately create sufficient strain, and hence stress, to impede further progress. Close examination of the displacement curves in Fig. 2a (see inset) also shows that at higher De the fluctuating component becomes smaller.

Figure 2b shows the swimmer positions and shapes for $De = 0$ (Newtonian), 1, and 5, at the final time $t = 20$. The $De = 1$ swimmer is the leader, with the $De = 0$ and 5 swimmers lagging and nearly tied despite the latter's substantially slower speed (see Fig. 4a). However, this positional tie is only due to the greater speed of the OB swimmer at earlier times, which decreased as the polymeric stresses approached their steady behavior. Figure 2b also shows that we are not solving a strictly kinematic swimming problem wherein the shape dynamics is rigidly prescribed, but are instead determined by the interaction of fluid stresses and the forces internal to the swimmer. By the providential near-tie of the swimmers we are able to make a visual shape comparison among them, and we see that the stroke profile for the $De = 5$ swimmer is considerably flattened, particularly at the tail, in comparison with the other two cases.
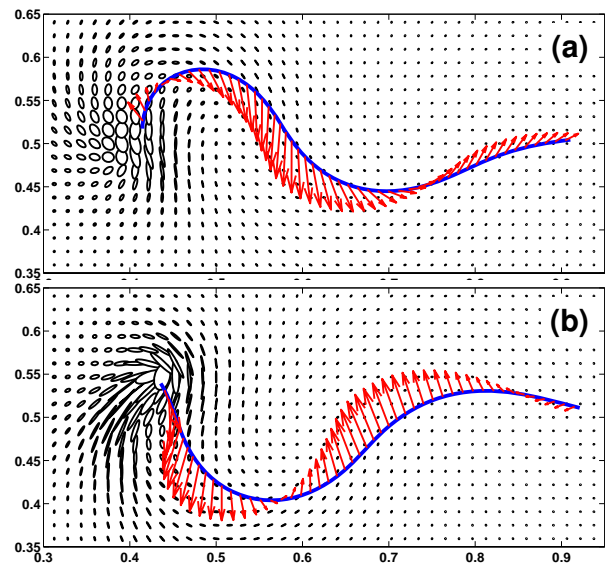
FIG. 3: Snapshots of the free swimmer for $De = 1$ at late times. The ellipses represent the (symmetric) polymeric stress tensor $\mathbf{S}$. The major axis is aligned with principal eigenvector of $\mathbf{S}$, with length scaled on the associated eigenvalue. The minor axis is associated with the second eigenvector/value pair of $\mathbf{S}$. As such, it represents the directions and degree of distension of the polymer field. The red vectors are the fluid velocity on Γ.

Figure 3 examines the spatial structure of the viscoelastic stresses during the swimming dynamics. The polymeric stress tensor $\mathbf{S}_p$ is symmetric and positive definite, and so has two positive eigenvalues, λ_1 and λ_2, and corresponding orthogonal unit eigenvectors $\mathbf{p}_1$ and $\mathbf{p}_2$. For $De = 1$, in the fluid surrounding the swimmer, we have plotted ellipses that visually represent the geometric structure of $\mathbf{S}_p$. The axes of each ellipse are aligned

with $\mathbf{p}_1$ and $\mathbf{p}_2$, and the axis lengths are scaled by λ_1 and λ_2. This visual diagnostic reveals how the polymer coils are being distended by the fluid flow. For example, $\mathrm{tr}(\mathbf{S}_p) = \lambda_1 + \lambda_2$ is an invariant of $\mathbf{S}_p$ and represents mean-square distension of the immersed polymer coils.

Figure 3a is at time $t = 19.73$, well after the swimmer has entered steady-state motion, and very near the time of peak forward velocity, which is nearly the same as for the Newtonian swimmer. A strong polymer stress concentration sits to the aft of the swimmer, associated with the strong straining of the fluid by the motion of the tail. At this time, the backward moving wave is reaching the end of the swimmer, and the tail is moving somewhat upwards. Figure 3b is at $t = 20$, about one-quarter stroke later (also interpretable as being one-quarter stroke earlier, with the figure flipped vertically). At this time, the rotation of the body about the tail has created a strong, anisotropic stress distribution there. An important fact is that while the swimmer is slipping backwards at this time, it is not slipping backwards as much as the Newtonian swimmer.
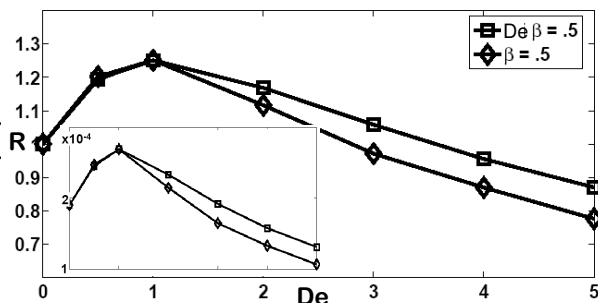
FIG. 4: As a function of De, the ratio $R(De)$ of average free swimmer speed to that of the Newtonian free swimmer. Inset: An estimate of swimming efficiency, $Eff= U^2/P$, versus De.

Efficiency is also an important aspect of swimming. For steady-state swimming we find that time-averaged input power, $P = \langle \int_\Gamma ds\, \mathbf{g} \cdot \mathbf{u}_\Gamma \rangle$, is nearly independent of De. This suggests that the point of maximal speed with respect to De is also the point of maximal effiency. This is borne out by Figure 4 whose inset plots the mechanical efficiency estimate $Eff= U^2/P$, where U is time-averaged x-velocity of the center of mass.

Discussion The main result of our study is that viscoelastic fluid response can actually increase the speed and efficiency of a simple undulatory swimmer. This increase is associated with highly strained fluid, sitting aft of the tail, which may be releasing hoop-like elastic stresses. While our study considers free swimmers and a full viscoelastic flow model, it remains idealized. Our swimmer is a two-dimensional sheet, not a three-dimensional swimmer like a spermatazoa. While nonlinear, the Oldroyd-B model is relatively simple, and is most appropriate for modeling a simple "Boger" fluid composed of a dilute suspension of high molecular weight polymers in a high viscosity solvent. While it captures elastic responses, it does not capture shear-thinning, nor the effects of finite length of distended polymers. It is unlikely that biological fluids such as mucus are so easily characterized. From the microscopic derivation of Oldroyd-B [11], the parameter $\beta \cdot Wi$ is interpreted as the ratio of polymer to solvent viscosity, which for many synthetic Boger fluids is an order one quantity (see, e.g. [13]), as we take it here.

There are aspects of experimental observation that we reproduce. Studying sperm swimming in a synthetic viscoelastic fluid medium Smith *et al.* [8] also find a greater displacement per beat (essentially our nondimensional velocity) than in a less viscoelastic medium. That said, this increase is more dramatic than in our study, and with real spermatazoa displacing more per beat by a factor of 2-3. This brings up another important point: real stroke forms (and frequencies) differ markedly depending upon the response properties of the medium, with waveforms being more concentrated near the tail for viscoelastic media (as we have tried to emulate here) [8, 14]. True swimming wave-forms reflect a balance between internally generated forces and the fluidic response and have been subject of study in Newtonian fluids [6, 15].

[1] S. Suarez and A. Pacey, Hum. Reprod. Update **12**, 23 (2006).
[2] L. Fauci and R. Dillon, Annu. Rev. Fluid. Mech. **38**, 371 (2006).
[3] S. Nakamura, Y. Adachi, T. Goto, and Y. Magariyama, Biophysical Journal **90**, 3019 (2006).
[4] G. I. Taylor, Proc. R. Soc. London, Ser. A **209**, 447 (1951).
[5] E. Lauga, Phys. Fluids **19**, 083104 (2007).
[6] H. Fu, T. Powers, and C. Wolgemuth, Phys. Rev. Lett. **99**, 258101 (2007).
[7] H. Fu, C. Wolgemuth, and T. Powers, Phys. Fluids **21**, 033102 (2009).
[8] D. Smith, E. Gaffney, H. Gadelha, N. Kapur, and J. Kirkman-Brown, Cell Mot. and the Cyto. **66**, 220 (2009).
[9] D. Wolf, L. Blasco, M. Khan, and M. Litt, Fertil. Steril. **32**, 166 (1979).
[10] C. Peskin, Acta. Numer. **11**, 479 (2002).
[11] R. Larson, *The Structure and Rheology of Complex Fluids* (Oxford University Press, 1998).
[12] L. J. Fauci and C. S. Peskin, J. Comput. Phys. **77**, 85 (1988).
[13] P. Arratia, C. Thomas, J. Diorio, and J. Gollub, Phys. Rev. Letters **96**, 144502 (2006).
[14] H. Ho and S. Suarez, Reprod. **122**, 519 (2001).
[15] R. Dillon, L. Fauci, and X. Yang, Computers and mathematics with applications **52**, 749 (2006).